Nanoscale

Accepted Manuscript

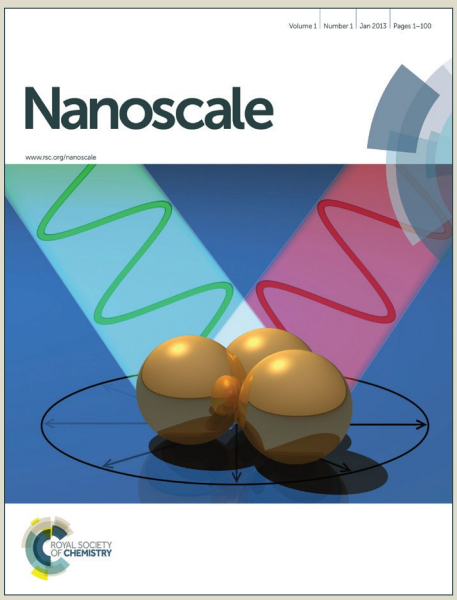

ROYAL SOCIETY OF CHEMISTRY

www.rsc.org/nanoscale

Journal Name

ARTICLE

DNA-inorganic hybrid nanovaccine for cancer immunotherapy

Guizhi Zhu[a], Yijing Liu[a], Xiangyu Yang[a], Young-Hwa Kim[a], Huimin Zhang[a], Rui Jia[b], Hsien-Shun Liao[c], Albert Jin[c], Jing Lin[c], Maria Aronova[c], Richard Leapman[c], Zhihong Nie[d], Gang Niu[a], and Xiaoyuan Chen[a,*]

Received 00th January 20xx,
Accepted 00th January 20xx

DOI: 10.1039/x0xx00000x

www.rsc.org/

Cancer evolves to evade or compromise the surveillance of immune system, and cancer immunotherapy aims to harness the immune system in order to inhibit cancer development. Unmethylated CpG dinucleotide-containing oligonucleotides (CpG), a class of potent adjuvants that activate the Toll-like Receptor 9 (TLR9) located in the endolysosome of many antigen-presenting cells (APCs), are promising for cancer immunotherapy. However, clinical application of synthetic CpG confront many challenges such as suboptimal delivery into APCs, unfavorable pharmacokinetics caused by limited biostability and short in vivo half-life, and side effects associated with leaking of CpG into the systemic circulation. Here we present DNA-inorganic hybrid nanovaccines (hNVs) for efficient uptake into APCs, prolonged tumor retention, and potent immunostimulation and cancer immunotherapy. hNVs were self-assembled from concatemer CpG analogs and magnesium pyrophosphate (Mg_2PPi). Mg_2PPi renders hNVs resistance to nuclease degradation and thermal denaturation, both of which are demanding characteristics for effective vaccination and the storage and transportation of vaccines. Fluorophore-labeled hNVs were tracked to be efficiently internalized into the endolysosomes of APCs, where Mg_2PPi was dissolved in acidic environment and thus CpG analogs were exposed from hNVs. Internalized hNVs in APCs led to 1) elevated secretion of proinflammatory factors, and 2) elevated expression of co-stimulatory factors. Compared with molecular CpG, hNVs dramatically prolonged the tissue retention of CpG analogs and reduced splenomegaly, a common side effect of CpG. In a melanoma mouse model, two injections of hNVs significantly inhibited the tumor growth and outperformed the molecular CpG. These results suggest hNVs are promising for cancer immunotherapy.

Introduction

The immune system evolves to be a comprehensive defense network protecting the host from a variety of diseases, including cancer. However, the immune system is often compromised in cancer patients by immunosuppressive tumor microenvironment[1] that lacks antitumor cytotoxic $CD8^+$ T cells and contains an excess of tumor-infiltrating lymphocytes (TILs), such as regulatory T cells and myeloid-derived suppressor cells. Consequently, these complications suppress anti-cancer immune responses, and promote immune evasion and oncogenesis[2]. However, current primary cancer treatment, such as surgery, chemotherapy, and radiotherapy, have limited efficacy to solve these complications. Alternatively, cancer immunotherapy attempts to normalize and harness the immune system to fight cancer.

Cancer immunotherapy has made substantial progress in the past decades. By leveraging the whole immune system, immunotherapy is especially promising for the treatment of recurrent cancer and metastatic cancer[3, 4]. Unmethylated cytosine-guanosine (CpG) motifs[5, 6] are the most potent immunostimulatory adjuvants known to date, and have been studied as adjuvants or vaccines for immunotherapy *via* pattern recognition-triggered immune response. Derived from pathogen-associated molecular patterns (PAMPs), CpG mimics pathogen genome and provides a "danger" signal to immune system, thereby triggering innate immune responses and facilitating adaptive immune responses[7]. Particularly, CpG activates the immune system by binding to Toll-like receptor 9 (TLR9) located in the endolysosome of many antigen-presenting cells (APCs)[7-9] and activating TLR9 signaling pathway, leading to the activation of transcription factor nuclear factor-kappaB (NF-κB) and mitogen-activated protein kinase (MAPK) pathways. These signaling pathways induce elevated expression of proinflammatory cytokines and chemokines (*e.g.*, tumor necrosis factor-α (TNF-α), interleukin 6 (IL-6), and IL-12)[10], upregulated expression of cell-surface co-stimulatory factors (*e.g.*, CD80 and CD86), promotion of the survival and proliferation of APCs, as well as promotion of Th1 immunostimulatory response and inhibition of Th2

[a] *Laboratory of Molecular Imaging and Nanomedicine, National Institute of Biomedical Imaging and Bioengineering (NIBIB), National Institutes of Health (NIH), Bethesda, MD 20892*
Email: shawn.chen@nih.gov; Tel: (+1) 301-451-4246
[b] *Section on Intracellular Protein Trafficking, Cell Biology and Metabolism Program, National Institute of Child Health and Human Development, NIH, Bethesda, MD 20892*
[c] *Laboratory of Cellular Imaging and Macromolecular Biophysics, NIBIB, NIH, Bethesda, MD 20892*
[d] *Department of Chemistry and Biochemistry, University of Maryland, College Park, MD 20742.*
Electronic Supplementary Information (ESI) available: supplemental materials and methods, characterization of hNVs. See DOI: 10.1039/x0xx00000x

immunoregulatory response in adaptive immune response[11]. CpG has been studied in a panel of clinical trials[12] for the immunotherapy of melanoma (*e.g.*, NCT00085189 and NCT00112229), metastatic breast cancer (*e.g.*, NCT00043394), and malignant glioblastoma (*e.g.*, NCT00190424), to name a few.

Nonetheless, the development of CpG-based cancer immunotherapy has been confronted with multiple challenges, mainly including unfavorable pharmacokinetics, systemic side effects, and inefficient intracellular delivery into APCs[13, 14]. For instance, with intrinsic negative charge, synthetic molecular CpGs have limited efficiency to be internalized into APCs for TLR9 recognition; yet, TLR9 are evolutionarily expressed within cells (on endolysosome membranes) for the detection of intracellular "foreign" molecules, such as pathogen DNA. Further, conventional molecular CpGs can only induce temporary immune responses, due to fast clearance, short tissue retention time, nuclease susceptibility, and intrinsically temporary innate immune responses induced by CpGs. Moreover, CpGs that have leaked into systemic circulation can stimulate B cells and plasmacytoid dendritic cells to express proinflammatory mediators and cause side effects. To address these challenges, current approaches include chemically modifying CpG[15-17] or incorporating CpG[18-25] into nanocarriers. Particularly, nanocarriers are potential to prolong the tissue retention time of loaded therapeutics, and to reduce exposure of CpG in systemic circulation.

Here we present the development of DNA-inorganic hybrid nanovaccines (hNVs) that are promising to solve the above complications. These hNVs were intrinsically implanted with CpG analogs and protective Mg_2PPi for cancer immunotherapy (scheme in Fig. 1). We have demonstrated efficient cell uptake of hNVs into two major types of APCs, dendritic cells and macrophages, and CpG analogs were exposed from uptaken hNVs in the endolysosome, leading to potent immunostimulation as evidenced by dramatically elevated secretion of proinflammatory factors and co-stimulatory factors. *In vivo* pharmacokinetic imaging proved prolonged tumor retention of hNVs in mice, and hNVs were further shown to have less systemic toxicity than molecular CpG counterpart. Tumor immunotherapy study demonstrated potent cancer immunotherapeutic efficacy of hNVs. Additionally, hNVs are featured with high loading capacity of CpG analogs, and high stability resulting from biomineralization of CpG analogs by Mg_2PPi. Collectively, these characteristics make hNVs promising for potent cancer immunotherapy.

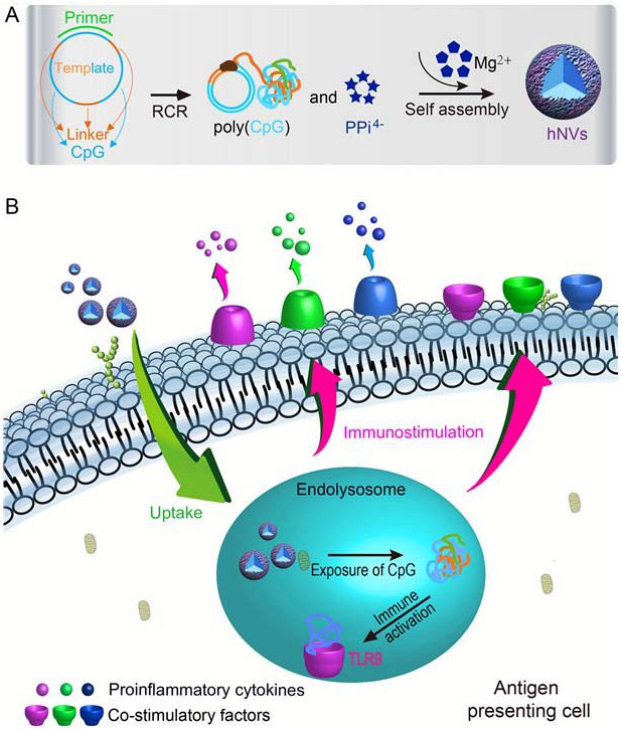

Fig. 1. Illustration of self-assembled hNVs for cancer immunotherapy. Spherical hNVs are self-assembled from the complexation of concatemer DNA CpG analogs and water-insoluble Mg2PPi via a single-step enzymatic reaction: RCR. Using a circular DNA template, RCR simultaneously produce a large amount of concatemer CpG analogs and pyrophosphate ions (PPi4-), the latter of which then combine with Mg2+ in buffer to form Mg2PPi. The CpG analogs and Mg2PPi are then co-precipitated to self-assemble into hNVs. hNVs are readily taken up into APCs, including dendritic cells and macrophages, and trigger the immune activation and maturation of these immune cells, leading to the secretion of proinflammatory cytokines and upregulation of maturation markers on cell surfaces. Compared to molecular CpG, hNVs have prolonged tissue retention time and reduced side effects. In a melanoma mouse model, hNVs potently inhibit tumor progression.

Results and Discussion

Construction and characterization of hNVs

Using Rolling Circle Replication (RCR),[26-29] hNVs were self-assembled in a one-step enzymatic reaction (Fig. 1). Particularly, a DNA template (sequences in Table S1) was designed to encode concatemer CpG analogs. This phosphorylated linear template was then circularized using T4 ligase and a ligation helper DNA that was complementary to part of both 3' and 5' ends of the linear template. This helper DNA was intentionally designed to also serve as the primer for subsequent RCR reaction. RCR utilized Φ29 DNA polymerase and the template to generate two essential composites of hNVs: long DNA integrated with a large amount of concatemer CpG as well as pyrophosphate ions (PPi^{4-}), as a result of the conversion of triphosphate deoxynucleotides to DNA. CpG 1826, a CpG known to have potent immunostimulatory activity in murine immune system[15], was used as a model in this study. Φ29 polymerase is well known for its efficient production of DNA, as such concatemer CpG analogs were efficiently synthesized. Meanwhile, by combining with a high

concentration of doped Mg^{2+} (10 mM) in the reaction buffer, the PPi^{4-} generated from RCR formed magnesium pyrophosphate (Mg_2PPi), which was insoluble in neutral-pH buffer and presumably co-precipitated with DNA, resulting in the self-assembly of flower-like hNVs.

The size of hNVs is readily tunable by simply controlling reaction time (Fig. S1). As observed using scanning electron microscopy (SEM), hNVs formed from 8-h RCR had an average diameter of ~1 μm (Fig. 2*A*), which was confirmed by using dynamic light scattering (DLS) (Fig. 2*B*) and atomic force microscopy (AFM) measurements (Fig. S2). Particles with diameters of up to 1 μm can be efficiently taken up by APCs such as macrophages and dendritic cells (DCs). Indeed, particles of these sizes are common in insoluble aluminum salts, the most common adjuvants in clinical use[30]. Therefore, we chose hNVs prepared from 8-h RCR for further study. Using the same method, GpC, which loses immunostimulatory capability by mutating the two *CG* dinucleotides in CpG-1826 into two *GC* dinucleotides (see sequences in Table S1), were incorporated into GpC DNA-inorganic hybrid nanoflowers (GpC-NFs, Fig. S3) as a control.

Given the versatile addressable sites on the DNA primer used in RCR, various functional moieties such as fluorophores or therapeutics can be chemically conjugated and subsequently incorporated into hNVs during hNV self-assembly. In this study, fluorophores were incorporated into hNVs (Fig. 2*C*) and the fluorophore-modified hNVs were used to monitor the behaviors of hNVs in cells and in mice. Since only one fluorophore was attached on one elongated DNA molecule generated from RCR, the intense fluorescence of hNVs implies that substantial copies of DNA products from RCR were incorporated into each hNV, indicating a high payload capacity of hNVs. To further quantify CpG analogs in hNVs, hNVs were first treated with EDTA, which chelated Mg^{2+} and led to dissolution of hNVs, as shown in SEM observation in Fig. S4. The remaining DNA in the solution was then purified by removing EDTA, Mg^{2+}, and PPi^{4-} using centrifugation filtration. The amount of the resulting DNA was estimated by measuring the absorbance at 260 nm and converting it to the equivalents of CpG. As a result, the template was estimated to be replicated for 15 times within 8 h, which is equivalent to 45 copies of CpG, given that 3 copies of CpG analogs were encoded by each DNA template. The presence of Mg_2PPi in hNVs was demonstrated by energy-dispersive X-ray spectroscopy (EDX) (Fig. 2*D*), which is consistent with previous reports[31, 32]. Indeed, the morphology of pure Mg_2PPi nanostructures formed by simple doping of Mg^{2+} and PPi^{4-} simulated that of hNVs (Fig. S5). The biocompatibility of hNVs was supported by their negligible cytotoxicity (Fig. S6). Indeed, both Mg^{2+} and PPi^{4-} are ubiquitous in human body, and many

Next, hNVs were evaluated *in vitro* for uptake into murine immune cells for TLR9 activation and immunostimulation. In murine host, CpG activates APCs, including macrophages, DCs, and B cells. CpG activation triggers the elevated secretion of proinflammatory cytokines (*e.g.*, TNF-α, IL-6, and IL-12) and upregulates expression of cell surface co-stimulatory factors (*e.g.*, CD80, and CD86)[11, 36]. Macrophage-like RAW264.7 cells were first studied for immunostimulation by hNVs. The ability of hNVs to be internalized into immune cells was first evaluated. After incubating RAW264.7 cells with Alexa488-labeled hNVs for 4 h, hNVs were colocalized with endolysosomes stained with Lysotracker Red DND-99, as examined by confocal microscopy (Fig. S8*A*). Given that TLR9 is located in the endolysosome of APCs[8, 9], the colocalization of hNVs and endolysosomes provides the basis for CpG analogs in hNVs to bind to TLR9 and then activate TLR9 signaling pathway for immunostimulation. The uptake of hNVs into these cells was also confirmed by flow cytometry (Fig. S8*B*). To evaluate hNVs-induced immunostimulation, RAW264.7 cells were incubated with hNVs, followed by determining the expression levels of co-stimulatory markers on cell surfaces and the level of secreted proinflammatory cytokines in cell culture medium. Flow cytometry analysis of the above-treated macrophages demonstrated that both hNVs and CpG specifically triggered the elevated expression of co-stimulatory factors, CD80 and CD86 on macrophages (Fig. 3*A* and Fig. S9*A*). In contrast, expression of these co-stimulatory factors were negligibly

analysis (Fig. S11*A*). Again, confocal microscopy revealed that Alexa488-labeled hNVs were efficiently taken up by BMDCs, and hNVs were co-localized with the endolysosomes in BMDCs (Fig. S11*B*). Flow cytometric analysis of BMDCs treated with hNVs demonstrated elevated expression of costimulatory factors CD80 and CD86 on BMDC surfaces (Fig. 3*C*). ELISA analysis demonstrated that BMDCs were specifically triggered to exhibit elevated secretion of TNFα, IL-6, and IL-12, in contrast to negligible elevation induced by control GpC-NFs (Fig. 3*D*). The immunostimulatory potency of hNVs was comparable to that of PS-CpG (Fig. 3*D*). Taken together, these results clearly demonstrated that hNVs were efficiently taken up into the endolysosome of these two representative APCs, and activated these cells to upregulate cell-surface costimulatory factors and release proinflammatory cytokines that are instrumental for cancer immunotherapy. Note that once hNVs are taken up into the endolysosome, it is critical for CpG analogs to be exposed from hNV complexes in order to bind to TLR9. It is hypothesized that the release of DNA from hNVs can be facilitated by the acidic environment of endolysosome (pH 4-6)[37], in consideration of increased solubility of Mg_2PPi in acidic environment. To test this hypothesis, hNVs were treated in buffer at pH 4 and pH 5, respectively, for 4 h. SEM results showed that the structures of hNVs were completely collapsed, indicating the degradation of Mg_2PPi scaffold and exposure of incorporated DNA (Fig. S12).

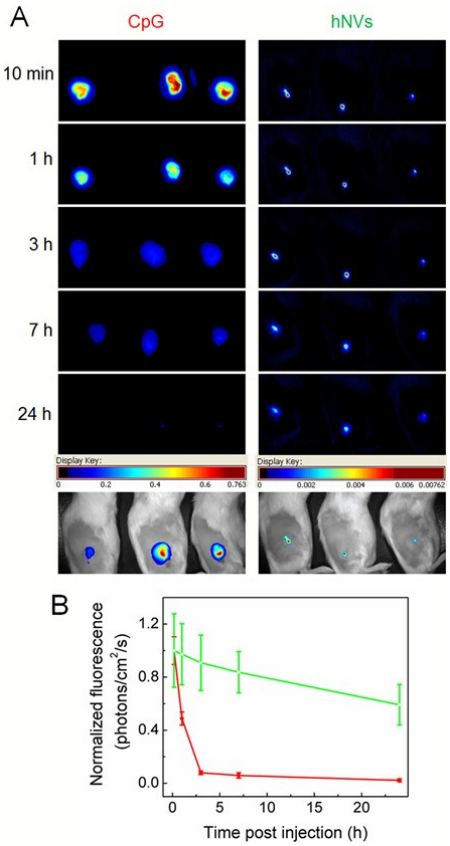

Fig. 4. Pharmacokinetic study of hNVs indicating prolonged tumor retention time of hNVs compared to molecular CpG. (A) IR800-labeled hNVs and CpG (PS backbone), respectively, were injected into subcutaneous B16F10 tumors at a dose of 1 nmol CpG equivalent per mouse. The pharmacokinetics of hNVs or CpG were monitored at the indicated time points by optical imaging. The difference of fluorescence intensities in CpG group and hNV group at the same time points was due to different amount of injected IR800 when the CpG amounts were equivalent in molecular CpG and hNVs (the amount of IR800 in CpG was 45 times of that in hNVs, because in hNVs, one IR800-labeled primer was linked with a RCR DNA product integrated with 45 CpG equivalent). Shown at the bottom are representative overlayed images of mice and fluorescence. (B) Quantification of normalized average fluorescence intensities in images shown in (A). Data represent mean ± s.e.m..

Prolonged tumor retention and reduced side effects of hNVs compared with molecular CpG

With potent *in vitro* immunostimulatory effect, hNVs were next evaluated in mice. The *in vivo* efficacy of conventional molecular CpG is often thwarted by unfavorable pharmacokinetics, namely short tissue retention, due to multiple reasons such as nuclease degradation as well as fast clearance. The short retention further causes short duration of immunostimulation and hence modest therapeutic efficacy. hNVs are promising to address this issue, in that CpG analogs are integrated within nanovehicles and protected from nuclease degradation or fast clearance. To study the tumor retention time of hNVs, IR800-labeled hNVs (SEM images in Fig. S13) was intratumorally injected into B16F10 melanoma tumor, followed by optical imaging. IR800-labeled molecular PS-CpG was used as a control. In contrast to relatively fast diffusion and clearance of molecular CpG, hNVs proved to prolong retention time in tumor (Fig. 4). The ability of hNVs to prolong tissue retention time can be attributed to the facts that the nano- to micro- scale vehicles can serve as a physical shield of incorporated DNA, and that the elongated DNA products from RCR reaction have much higher molecular weights. Both of these facts can protect the integrated DNA from fast degradation or clearance. The prolonged tumor retention time of hNVs is expected to prolong the immunostimulation and thus increase immunotherapeutic efficacy.

Consistent with the short tissue retention, another drawback of conventional molecular CpG is associated with multiple systemic side effects caused by CpG drained into systemic circulation[13, 14]. One of these side effects is splenomegaly associated with extramedullary haematopoiesis[14]. To evaluate hNVs for this side effect, hNVs and molecular CpG were subcutaneously injected into mice, followed by determination of the size and weight of spleens to assess splenomegaly. Results revealed that hNVs greatly reduced splenomegaly compared to the molecular CpG counterparts, which clearly indicates the reduction of systemic side effects by hNVs (Fig. 5). Furthermore, H&E staining of spleens in vaccinated mice further confirmed the

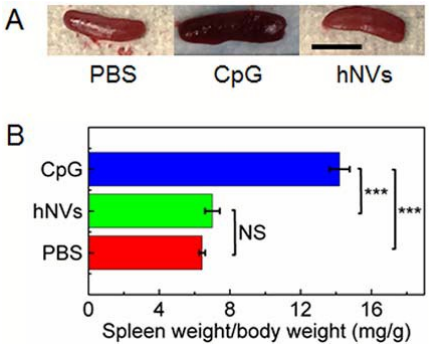

Fig. 5. hNVs reduced side effects (splenomegaly) compared with molecular CpG. (A) Representative images of spleens from mice subcutaneously injected with PBS, CpG, and hNVs, respectively. Spleens were collected on day 6 post treatment. (B) Quantification of the ratios of mouse spleen weights over body weights showing significant reduction of splenomegaly in mice treated with hNVs compared with that of CpG. Asterisks represent significant differences between weight ratios of mice treated with the corresponding different regimes (***p<0.001, n = 3 mice/group; one-way ANOVA with Bonferroni post test). Data represent mean ± s.e.m. NS, not significant.

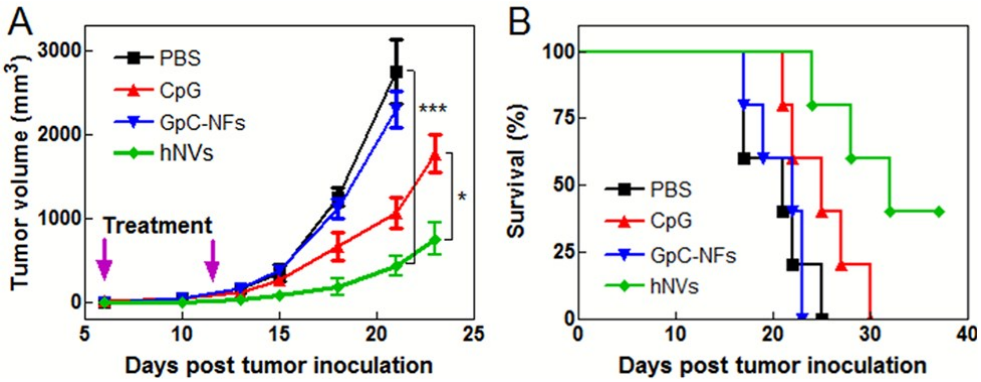

Fig. 6. hNVs-mediated cancer immunotherapy in a B16F10 melanoma mouse model. (A) Tumor volumes on mice treated with PBS, molecular CpG, control GpC-NFs, or hNVs at the dosage of 2 nmol CpG equivalent per mouse, by intratumoral injection on day 6 and day 12 post tumor inoculation. Asterisks represent significant differences between tumor volumes in mice treated with the corresponding different regimes (***p<0.001, *p<0.1, n = 5 mice/group; one-way ANOVA with Newman–Keuls post test). Data represent mean ± s.e.m.. (B) Kaplan–Meier survival curve of mice treated with the above regimes.

biocompatibility of hNVs (Fig. S14).

Potent tumor immunotherapeutic efficacy induced by hNVs

Finally, hNVs were evaluated for cancer immunotherapy in a tumor model of melanoma, the most aggressive and dangerous form of skin cancer in the United States. On day 6 post inoculation of B16F10 tumor, at which time tumors were palpable (*ca.* 50 mm^3), mice were randomly divided into four groups and each group were respectively treated with 1) PBS, 2) free CpG, 3) GpC-NFs, and 4) hNVs, at a dose of 2 nmol equivalent CpG per mouse by intratumoral injection. The treatment was repeated on day 12 post tumor inoculation. As a result, hNVs specifically inhibited tumor growth, in contrast to weak to negligible inhibition by other regimes (Fig. 6*A*). Consistent with tumor growth inhibition, hNVs-treated mice showed the highest survival rate, with 2 out of 5 mice alive after 37 days of treatment, which is significantly higher than mice treated with other regimes (Fig. 6*B*). During the course of treatment, hNVs-treated mice did not exhibit any illness or significant weight change, which further evidences the high biocompatibility of hNVs (Fig. S15). Altogether, these results demonstrated potent therapeutic efficacy and reduced side effects of hNVs, making them a novel and robust platform for cancer immunotherapy.

Conclusion

In summary, we present here a novel nanovaccine based on DNA-inorganic hybrid nanostructures. These hNVs are featured by: 1) simple preparation and programmable "implantation" of a high payload capacity of immunotherapeutic CpG analogs, 2) chemically addressable sites allowing for labeling with additional theranostic agents, 3) high stability as dry powder, under thermal denaturation, or under physiological environment, 4) efficient uptake into APCs, and conditional exposure of CpG analogs from hNVs, 5) potent immunostimulatory effect; 6) prolonged tumor retention time and hence improved pharmacokinetics compared with molecular CpG, 7) reduced side effects and high biocompatibility, and 8) potent antitumor immunotherapeutic efficacy. Future investigation of hNVs can include detailed dissection of the mechanism of immunostimulation, as well as combination of hNVs-based immunotherapy with tumor-specific antigens or chemotherapy. Taken together, these features make hNVs promising for cancer immunotherapy.

Experimental Section

Synthesis of hNVs

DNA nanoflowers, including hNVs, were synthesized using rolling circle replication (RCR). Particularly, linear 5'-phosphorylated DNA templates (0.6 μM) were circularized using ligation helper DNA (1.2 μM) and T4 DNA ligase (10 U/μL; New England Biolabs, Ipswich, MA). This ligation helper DNA also served as the primers in subsequent RCR in reaction solution containing circularized template (0.3 μM), Φ29 DNA polymerase (2 U/μL; New England Biolabs, Ipswich, MA), 2 mM/μL dNTP, and 1x BSA in buffer solution (50 mM Tris-HCl, 10 mM $(NH_4)_2SO_4$, 10 mM $MgCl_2$, and 4 mM Dithiothreitol). RCR was carried out at 30 °C for a specified time. Reaction was terminated by deactivating Φ29 at 90 °C for 10 min. If applicable, fluorophores (Alexa488 or IR800) were chemically labeled on the 5' ends of primers used for RCR, in order for the resulting nanostructures to be intrinsically labeled with fluorophores. The resulting products were washed and precipitated using Dulbecco's PBS for three times, stored at 4 °C if necessary, and were resuspended in Dulbecco's PBS before use.

Characterization of hNVs

The sizes and morphologies of nanomaterials were characterized using scanning electron microscopy (SEM) and atomic force microscopy (AFM). SEM samples were prepared by depositing the above-prepared samples onto conductive glass, following by drying, washing with double-distilled H_2O (diH_2O) and further drying. Samples were coated with Au (5 nm) by spray, and observed on an S-4800 scanning electron microscope. For AFM of hNVs, samples (10 μL) were casted on freshly peeled mica substrate, followed by drying, rinsing, and dehumidifying. AFM was carried out in tapping-mode in air on a PicoForce Multimode AFM (Bruker, CA) equipped with a Nanoscope® V controller, a type E scanner head, and an OTESPA (Bruker, CA) AFM cantilever. AFM images were then analyzed by Nanoscope Software (ver. 7.3-8.15, Bruker, CA). The sizes of hNVs suspended in Dulbecco's PBS were also characterized using dynamic light scattering (DLS) on a Nanoparticle Analyzer (HORIBA Scientific, Tokyo, Japan). Bright field or fluorescence images of fluorophore-labeled hNVs were taken on a Zeiss LSM 780 confocal microscope (Chesterfield, VA).

Isolation and culture of bone marrow derived dendritic cells (BMDCs)

BMDCs were isolated from femur bones of C57BL/6J mice (The Jackson Laboratory). BMDCs were cultured in RPMI-1640 medium supplemented with 10% heat-inactivated FBS, 100 U/mL penicillin, 100 μg/mL streptomycin, and 20 ng/mL GM-CSF (PeproTech, Rocky Hill, NJ), in a cell culture incubator with 5% CO_2 at 37 °C. Fresh cell culture medium and GM-CSF were added into BMDCs after culturing for 3 days. Non-adherent and loosely adherent immature DCs were harvested at day 6 post isolation from bone marrow and phenotyped by determining expression of CD11c using flow cytometry.

***In vitro* immunoactivation**

In vitro immunoactivation was characterized using flow cytometry and enzyme-linked immunosorbent assay (ELISA). Flow cytometry was used to study the expression levels of costimulatory markers and maturation markers. Particularly, RAW264.7 cells or BMDC cells were seeded into 24-well plate, and one day later, cells were treated with hNVs or the corresponding control regimens at the specified concentrations for 24 h before cell detaching and washing. Cells were resuspended in Dulbecco's PBS and incubated with anti-CD11c-FITC, anti-CD80-PerCP, or anti-CD86-FITC, (PeproTech, Rocky Hill, NJ) respectively, for 0.5 h on ice. Cells were then washed with Dulbecco's PBS for three times for flow cytometric analysis using a BD Beckman Coulter flow cytometer (Brea, CA). Results were analyzed using FlowJo Software (TreeStar, Ashland, OR). Alternatively, enzyme-linked immunosorbent assay (ELISA) was used to measure the concentration of secreted proinflammatory cytokines by immune cells upon immunoactivation. RAW264.7 cells or BMDCs were treated respectively with hNVs or the control regimes at the specified concentrations for 14 h. Cell culture medium was then collected and centrifuged to remove any debris. The concentrations of cytokines (e.g., TNF-α, IL-6, and IL-12) in the culture medium of RAW264.7 cells or BMDCs were assayed using ELISA (Life Technologies, Carlsbad, CA) as per manufacturer's instructions.

Evaluation of spleen side effects in mice

The ability of hNVs to induce splenomegaly was first evaluated. Particularly, C57BL/6J mice (3/group, The Jackson Laboratory) were intramuscularly (on thigh muscle) injected with 50 μL of PBS, CpG, and hNVs, respectively, at the dosage of 4 nmole/mouse of CpG or equivalent on day 0 and day 3, respectively. Mice were killed on day 6, and spleens were collected for further analysis. The spleen weights were determined and normalized to body weights. Results were statistically analyzed using Origin Software (Northampton, MA). Collected spleens were fixed in They were fixed in a Z-fix solution (Anatech Ltd., Battle Creek, MI) at room temperature. Haematoxylin and eosin (H&E) staining of spleens was performed and the slides were observed using a BX41 bright field microscope (Olympus, Shinjuku, Tokyo, Japan).

***In vivo* optical imaging of the pharmacokinetics of hNVs**

In vivo imaging of the pharmacokinetics of CpG or hNVs was performed in a B16F10 melanoma tumor model inoculated in Blab/c mice (3/group, The Jackson Laboratory). Particularly, 5 x 10^5 B16F10 cells were inoculated subcutaneously into mice. On day 10 post-inoculation, mice were intratumorally administered with IR800-labeled CpG or IR800-labeled hNVs at the dosage of 1 nmole/mouse of CpG or CpG equivalents in hNVs. The fluorescence of the resulting mice were recorded on a Maestro II *in vivo* imaging system (Caliper Life Sciences, Hopkinton, MA) at specified time points after injection. Region of interest (ROI) was drawn to include the fluorescent regions and the average fluorescence intensity of the ROI was analyzed for quantification.

Cancer immunotherapy.

C57BL/6J mice (The Jackson Laboratory) were housed in an animal facility under pathogen-free conditions. A xenograft B16F10 melanoma tumor model was used for the study of hNV-based immunotherapy. Specifically, 5 x 10^5 B16F10 cells were inoculated subcutaneously into mice. Mice were treated with specified regime on day 5 and day 10 post-inoculation by intratumoral injection of 2 nmole/mouse of CpG or equivalents (5 mice/group). Mouse weights and tumor sizes were continuously monitored. Tumor volume was calculated using the following formula:

$$\text{Volume} = (\text{length}*\text{width}^2)/2$$

Mice were killed when any dimensions of tumor exceeded 2 cm or when tumor developed necrosis or ulceration. All animal work was conducted in appliance to the NIH Guide for the Care and Use of Animals under protocols approved by the NIH Clinical Center Animal Care and Use Committee. Results were analyzed using GraphPad Prism 4 (La Jolla, CA).

Acknowledgements

This work was supported by intramural research program of the National Institute of Biomedical Imaging and Bioengineering (NIBIB), National Institutes of Health (NIH).

References

1. K. Palucka and J. Banchereau, *Nat. Rev. Cancer*, 2012, **12**, 265-277.
2. B. Thomas, G. C. Pierre, G. Eli and M. J. Elizabeth, *Nat. Rev. Cancer*, 2012, **12**, 307-313.
3. S. A. Rosenberg, J. C. Yang and N. P. Restifo, *Nat. Med.*, 2004, **10**, 909-915.
4. P. Sharma and J. P. Allison, *Science*, 2015, **348**, 56-61.
5. D. M. Klinman, *Nat. Rev. Immunol.*, 2004, **4**, 249-258.
6. G. Hartmann, G. J. Weiner and A. M. Krieg, *Proc. Natl. Acad. Sci. USA*, 1999, **96**, 9305-9310.
7. M. B. Gregory, C. K. Jonathan and M. Ruslan, *Nat. Immunol.*, 2005, **7**.
8. A. Chockalingam, J. C. Brooks, J. L. Cameron, L. K. Blum and C. A. Leifer, *Immunol. Cell Biol.*, 2008, **87**, 209-217.
9. E. Latz, A. Schoenemeyer, A. Visintin, K. A. Fitzgerald, B. G. Monks, C. F. Knetter, E. Lien, N. J. Nilsen, T. Espevik and D. T. Golenbock, *Nat. Immunol.*, 2004, **5**, 190-198.
10. D. M. Klinman, A. K. Yi, S. L. Beaucage, J. Conover and A. M. Krieg, *Proc. Natl. Acad. Sci. USA*, 1996, **93**, 2879-2883.
11. A. M. Krieg, *Nat. Rev. Drug Discov.*, 2006, **5**, 471-484.
12. J. Scheiermann and D. M. Klinman, *Vaccine*, 2014, **32**, 6377-6389.
13. T. Storni, C. Ruedl, K. Schwarz, R. A. Schwendener, W. A. Renner and M. F. Bachmann, *J. Immunol.*, 2004, **172**, 1777-1785.
14. T. Sparwasser, L. Hültner, E. S. Koch, A. Luz, G. B. Lipford and H. Wagner, *J. Immunol.*, 1999, **162**, 2368-2374.
15. H. Liu, K. D. Moynihan, Y. Zheng, G. L. Szeto, A. V. Li, B. Huang, D. S. Van Egeren, C. Park and D. J. Irvine, *Nature*, 2014, **507**, 519–522.
16. H. Liu, B. Kwong and D. J. Irvine, *Angew. Chem. Int. Ed.*, 2011, **50**, 7052-7055.
17. D. J. Irvine, M. A. Swartz and G. L. Szeto, *Nat. Mater.*, 2013, **12**, 978-990.
18. P. Zhang, Y.-C. C. Chiu, L. H. Tostanoski and C. M. Jewell, *ACS Nano*, 2015, **9**, 6465-6477.
19. J. I. Darrell, C. H. Melissa, R. Kavya and T. Talar, *Chem. Rev.*, 2015, 2018197663.
20. D. A. Titta, M. Ballester and Z. Julier, *Proc. Natl. Acad. Sci. USA*, 2013.
21. D. N. Nguyen, K. P. Mahon, G. Chikh, P. Kim, H. Chung, A. P. Vicari, K. T. Love, M. Goldberg, S. Chen, A. M. Krieg, J. Chen, R. Langer and D. G. Anderson, *Proc. Natl. Acad. Sci. USA*, 2012, **109**, E797-E803.
22. X. Liu, Y. Xu, T. Yu, C. Clifford, Y. Liu, H. Yan and Y. Chang, *Nano Lett.*, 2012, **12**, 4254-4259.
23. J. H. Kim, Y.-W. Noh, M. B. Heo, M. Y. Cho and Y. T. Lim, *Angew. Chem. Int. Ed*, 2012, **51**, 9670-9673.
24. M. Nishikawa, Y. Mizuno, K. Mohri, N. Matsuoka, S. Rattanakiat, Y. Takahashi, H. Funabashi, D. Luo and Y. Takakura, *Biomaterials*, 2011, **32**, 488-494.
25. J. Li, H. Pei, B. Zhu, L. Liang, M. Wei, Y. He, N. Chen, D. Li, Q. Huang and C. Fan, *ACS Nano*, 2011, **5**, 8783-8789.
26. G. Zhu, R. Hu, Z. Zhao, Z. Chen, X. Zhang and W. Tan, *J. Am. Chem. Soc.*, 2013, **135**, 16438-16445.
27. J. B. Lee, J. Hong, D. K. Bonner, Z. Poon and P. T. Hammond, *Nat. Mater.*, 2012, **11**, 316-322.
28. L. Zhang, G. Zhu, L. Mei, C. Wu, L. Qiu, C. Cui, Y. Liu, I. T. T. Teng and W. Tan, *ACS Appl. Mater. Interfaces*, 2015.
29. Y. Lv, R. Hu, G. Zhu, X. Zhang, L. Mei, Q. Liu, L. Qiu, C. Wu and W. Tan, *Nat. Protoc.*, 2015, **10**, 1508-1524.
30. F. A. Sharp, D. Ruane, B. Claass, E. Creagh, J. Harris, P. Malyala, M. Singh, D. T. O'Hagan, V. Pétrilli, J. Tschopp, L. A. O'Neill and E. C. Lavelle, *Proc. Natl. Acad. Sci. USA*, 2009, **106**, 870-875.
31. Y. H. Roh, J. B. Lee, K. E. Shopsowitz, E. C. Dreaden, S. W. Morton, Z. Poon, J. Hong, I. Yamin, D. K. Bonner and P. T. Hammond, *ACS Nano*, 2014, **8**, 9767-9780.
32. E. S. Kevin, R. Young Hoon, J. D. Zhou, W. M. Stephen and T. H. Paula, *Small*, 2014, **10**, 1623-1633.
33. FDA, 2011. *GRAS Notice 000383*
34. FDA, 2011. *Agency Response Letter GRAS Notice No. GRN 000383*
35. N. Fogh-Andersen, B. M. Altura and B. T. Altura, *Clin. Chem.*, 1995.
36. D. P. Sester, K. Brion, A. Trieu, H. S. Goodridge, T. L. Roberts, J. Dunn, D. A. Hume, K. J. Stacey and M. J. Sweet, *J. Immunol.*, 2006, **177**, 4473-4480.
37. H. Appelqvist, P. Wäster, K. Kågedal and K. Öllinger, *J Mol. Cell Biol.*, 2013, **5**, 214-226.